ues smaller than a certain baseline are set to zero. The values of the remaining pixels are binarized. The resultant image contains most of the spatial information existing within the original image; however, it is represented by fewer pixels and by only one bit per pixel.

The first category of digital image converters also includes important algorithms, which are commonly grouped together under the name *image enhancement* and include operators such as edge enhancement, noise filtering, sharpening, and magnifying. An important technique of image enhancement is contrast stretching. In this application, each gray level in the image is mapped by a predetermined rule into another gray level. A specific example is the histogram equalization method, where the input gray levels are mapped such that the output's gray level histogram is uniform. Such a distribution of gray levels helps to emphasize details of low contrast that could have not been seen before this operation took place. Mathematically such an operation may be described as:

$$v = f(u) = \sum_{x_i=0}^{u} \frac{h(x_i)}{\sum_{i=0}^{L-1} h(x_i)}$$

$$v' = \mathrm{Int}\left[\frac{v - v_{\min}}{1 - v_{\min}}(L-1) + 0.5\right]$$

where u represents a pixel value in the original image that has L gray levels x_i ($i = 0, 1, \ldots L-1$); $h(x_i)$ is the histogram of the original image (the number of pixels with gray level value x_i); $v_{\min}$ is the smallest value of v and Int is the integer value taking operation; v' is the output image, which is approximately uniformly distributed with L gray levels.

The last digital operation for image conversion that we wish to mention in this section is the region of interest (ROI) finding algorithms. In many applications, including point target detectors or electrooptical trackers, one needs algorithms to determine the reduced regions of the image that are relevant to the observer. After allocating the regions of interest, different operations of image conversion may be applied, according to the specific application discussed. Thus, in these types of applications, a smart digital image converter is involved since it first allocates a certain region of interest within the image and then applies a desired operation. These ROI algorithms may belong to the two mentioned categories, depending on the a priori information at hand.

The previously mentioned digital image conversion operations and other operations are explained in detail in Refs. 1 and 2. In the next sections we address optical and electrooptical techniques for image conversions.

OPTICAL AND ELECTROOPTICAL IMAGE CONVERTERS

An ordinary image is a representation of the luminance distribution of points (or pixels) of objects (for example, ordinary pictures taken by a camera) or a representation of absorption or reflection distributions of such objects. In this article, an image is any two-dimensional function that bears some information about an object. An image can be stored in many ways, for example, as a digital set of numbers in a two-dimensional array in a computer database file or on photographic film as the transmittance of each point.

Image converters that perform certain operations on images may be classified into two main categories. The first category deals with smart digital image processing algorithms. The second category is related to coordinate transformations, which are usually easily implemented by optical or electrooptical measures.

The first category includes image transforms such as the Fourier, Haar, wavelet, Hilbert, and Hartly transforms. These transformations are especially useful for image restoration (noise removal) and image analysis. A special application of image transforms is related to image compression. There are many techniques of compression; however, the one that is more relevant to image conversion is the discrete cosine transform (DCT) based method (JPEG). In this method the original image is divided into several kernels (subimages), whereby each kernel is transformed by a special spatially compressing transform (for instance, the DCT). The next step is to perform a threshold operation in which pixels with val-

SIMPLE OPTICAL CONVERTERS

Prisms

The prism is a basic optical element based on the principle of refraction; that is, light passing through a material gains a phase, which is proportional to the path length and the refractive index on that path. By varying the path length along adjacent trajectories, one may generate a desired phase slope.

A prism is a light-transmitting material having a slanted edge that generates a linear phase shape to a light beam

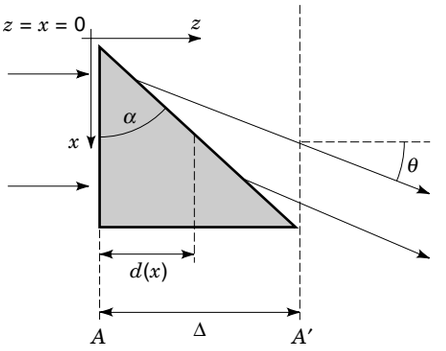

Figure 1. Light passing through a prism.

passing through it. Mathematically, one may express the path length within the prism as (see Fig. 1)

$$d(x) = x \tan \alpha \tag{1}$$

We should recall that a plane wave propagating in an arbitrary direction in free space may be expressed as:

$$f(\bar{r}) = A \exp[i\bar{k} \cdot \bar{r}] \tag{2}$$

where A is a constant coefficient, $\bar{r} = [x, y, z]$ is the location vector and $\bar{k} = [k_x, k_y, k_z]$ is the k vector of that plane wave. The k vector points to the direction of propagation, and its length is

$$|\bar{k}| = \frac{2\pi}{\lambda} \tag{3}$$

where λ is the wavelength of the propagating light. The phase front of a beam propagating in the z direction through a prism (Fig. 1) accumulates a phase up to plane A', given by

$$\phi = \frac{2\pi}{\lambda}\{nd(x) + [\Delta - d(x)]\} \tag{4}$$

where n is the refractive index of the prism's material. Taking out constant phase terms and rewriting the last expression yields

$$\phi = \frac{2\pi}{\lambda}(n-1)d(x) = \frac{2\pi}{\lambda}[(n-1)\tan\alpha]x = k_x x \tag{5}$$

The k_x term expresses the k vector projection into the x direction of the outgoing beam. Thus, if before the entrance into the prism the light had a k vector pointing only to the z direction, now a component of propagation to the x direction is developed. Denoting by θ the angle of propagation into the x direction (Fig. 1), one may write

$$k_x = \frac{2\pi}{\lambda}\sin\theta \tag{6}$$

where $\sin\theta = (n-1)\tan\alpha$. The k vector into the z direction now becomes

$$k_z = \frac{2\pi}{\lambda}\cos\theta \tag{7}$$

Thus, the prism element produces a change in the direction of propagation related to its corner angle α and the index of refraction n. This simple conversion of light does not have to be uniform over the entire beam. One may choose a set of prisms affecting the phase locally according to the relations previously mentioned and thus create an overall conversion of the input light-shaped image into a predetermined output phase front.

Lenses

A thin lens is another example of a basic refractive optical element that may be used to create optical phase front conversion, resulting in new beam behavior. An illustration of a lens may be seen in Figure 2.

Since the outer boundaries describing the lens shape are spherical functions (i.e., $x^2 + y^2 + z^2 = R^2$) the phase gained by an impinging plane beam, initially propagating to the z direction, passing from plane A to A' is

$$\phi = \frac{2\pi}{\lambda}[\Delta_0 + (n-1)\Delta(x,y)] \tag{8}$$

where

$$\Delta(x,y) = \Delta_0 - (R - \sqrt{R^2 - x^2 + y^2}) \tag{9}$$

Since R (the radius of the spherical surface) is much larger than x and y maximal values, one may approximate

$$z = \sqrt{R^2 - x^2 - y^2} = R\sqrt{1 - \frac{x^2+y^2}{R^2}} \approx R\left(1 - \frac{x^2+y^2}{2R^2}\right) \tag{10}$$

which leads to

$$\phi = -\frac{2\pi}{\lambda}\left[\frac{x^2+y^2}{2R}(n-1) - n\Delta_0\right] \tag{11}$$

The elimination of the constant phase factor yields

$$\phi = -\frac{2\pi}{\lambda}\left[\frac{x^2+y^2}{2R}(n-1)\right] = -\frac{\pi(x^2+y^2)}{\lambda F} \tag{12}$$

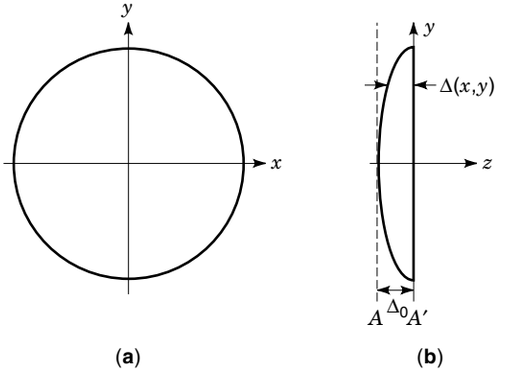

Figure 2. Lens profile: (a) x–y plane cross section, (b) y–z plane cross section.

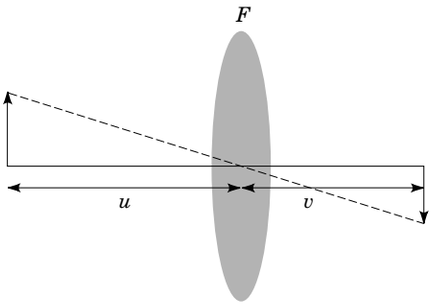

Figure 3. Imaging lens.

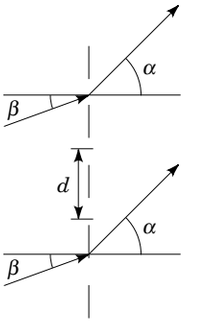

Figure 5. Diffraction grating.

where F is the focal length of the lens. Thus, apart from a constant phase multiplier, the phase transformation gained by the lens may be written as

$$t_1(x,y) = \exp\left[-i\frac{k}{2F}(x^2+y^2)\right] \tag{13}$$

Using geometrical ray considerations, or the Fresnel approximation from the theory of diffraction, which characterizes the propagation of light in free space, one may determine that a plane wave illuminating a lens is focused into a bright spot of light at distance F from the lens. The size of the spot is inversely proportional to the lens diameter. The plane at which this spot is obtained is called the back focal plane. The use of this property of the lens is most important for the design of optical image converters. First, by using an array of small lenses one may generate an array of spots obtained in the back focal plane of such composite lens. Second, a lens may be used as an imaging device. An object located at a distance u from the lens plane is imaged in a plane located a distance v behind the lens (see Fig. 3), where v satisfies the following relation:

$$\frac{1}{u}+\frac{1}{v}=\frac{1}{F} \tag{14}$$

An important feature of imaging, which is also seen in Figure 3 is that the image is inverted; that is, an object whose intensity profile is $f(x, y)$ is imaged as $f(-x, -y)$. Thus, an image conversion of 180° rotation is obtained.

Mirrors

A mirror is a light-reflecting element (see Fig. 4). Actually most of the existing elements in nature have the ability to partially reflect illumination. The uniqueness of a mirror is that it reflects almost all the light that illuminates it. The precise amount of reflection and transmission (Fresnel's coefficients) depends upon the polarization of the incident beam (polarization implies the direction of the electric component of the electromagnetic field with respect to the reflecting surface and the propagation direction), angle of incidence, and material's properties.

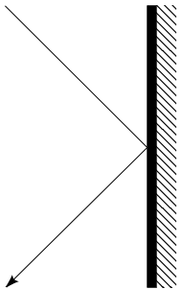

Figure 4. Mirror.

Once again, by forming an array of mirrors one may direct the light reflections in a predesigned manner and form a desired image conversion.

OPTICAL COORDINATE TRANSFORMATION—ANALYTICAL APPROACHES

An important feature of image conversion is the use of optical coordinate transformation techniques. By performing a desired coordinate transformation, a desired image conversion is obtained. In this section we describe four major analytical approaches to obtain coordinate transformations using optical or electrooptical modules. Then, we compare the techniques.

Multifacet

The multifacet approach (3,4) is a technique based on the fact that light passing through a grating changes its direction of propagation according to the following equation:

$$d\sin\beta \pm m\lambda = d\sin\alpha \tag{15}$$

where m is an integer number, d is the period of the grating, β is the angle of incidence, and α is the angle of the new direction of propagation (see Fig. 5).

Note that, in contrast to prisms, which also change light's direction of propagation, the grating is an element based on diffraction rather than refraction. The change in the propagation direction is not due to the thickness of the element but rather to its spatial frequency.

A far-field approximation of the Fresnel diffraction formula (also called a Fraunhofer approximation) may be expressed (apart from a constant multiplier and quadratic phase factor) as

$$g(x;z) = \int_{-\infty}^{\infty} g(x_0, z=0)\exp\left(\frac{-2\pi i x x_0}{\lambda z}\right)dx_0 \tag{16}$$

where $g(x; z)$ is the far-field Fraunhofer approximation and z is the distance between the output plane and the input plane. Since one recalls that the Fourier transform definition is

$$G(\nu) = \int_{-\infty}^{\infty} g(x) \exp(-2\pi i x \nu)\, dx \tag{17}$$

where $g(x)$ is the input function and $G(\nu)$ represents its Fourier transform, it is readily observed that the Fraunhofer approximation is a scaled Fourier transform of the input plane

$$g(x; z) = G\left(\frac{x}{\lambda z}\right) \tag{18}$$

If we examine the far-field expression for a plane wave illuminating a diffraction grating having a period of d and a transmittance given by the phase function $\exp(2\pi i x_0/d)$, one may easily obtain (when ignoring the finite extent of the grating):

$$g(x; z) = \int_{-\infty}^{\infty} \exp\left(\frac{2\pi i x_0}{d}\right) \exp\left(\frac{-2\pi i x x_0}{\lambda z}\right)\, dx_0 = \delta\left(\frac{x}{\lambda z} - \frac{1}{d}\right) \tag{19}$$

where $\delta(x)$ is Dirac's delta function, which vanishes everywhere except for $x = 0$ where it tends to infinity such that its area remains equal to unity. In our case the spot of light appears at $x = \lambda z/d$. The chosen input grating pattern has a phase dependence that varies linearly with the coordinate x, thus physically representing a prism. An arbitrary periodic object that has a periodicity d can be expanded via Fourier expansion series into terms exhibiting phase dependence $\exp(2\pi i m x_0/d)$, so that the far-field approximation consists of contributions appearing at

$$x \approx z \sin\alpha_m = \frac{\lambda z m}{d} \rightarrow d \sin\alpha_m = \lambda m, m = \cdots -2, -1, 0, 1, 2, \ldots \tag{20}$$

Note that Eq. (20) coincides with Eq. (15) when $\beta = 0$.

We now examine the two-dimensional case; a plane wave impinging upon a two-dimensional diffractive grating defined by a phase function $\exp\{2\pi i[(x/d_x) + (y/d_y)]\}$, becomes in the far-field,

$$\begin{aligned} g(x, yz) &= \iint \exp\left[2\pi i \left(\frac{x_0}{d_x} + \frac{y_0}{d_y}\right)\right] \\ &\quad \exp\left[-2\pi i \frac{x_0 x + y_0 y}{\lambda z}\right]\, dx_0\, dy_0 \\ &= \delta\left(\frac{x}{\lambda z} - \frac{1}{d_x}, \frac{y}{\lambda z} - \frac{1}{d_y}\right) \end{aligned} \tag{21}$$

The last expression means that light illuminating a certain grating is converted into a bright spot located at $x = \lambda z/d_x$, $y = \lambda z/d_y$. Note that the shift amount $x = \lambda z/d_x$, $y = \lambda z/d_y$ is determined by the spatial periods of the grating in the horizontal and vertical axes, d_x and d_y, respectively.

Assigning a different grating to each pixel in the input scene, image conversion may thus be obtained. This is due to the fact that associating a grating (d_x, d_y) to a pixel located in (x_m, y_m) will result in a bright spot located in the output plane (the far field) at $(\lambda z/d_{xm}, \lambda z/d_{ym})$ when d_{xm} and d_{ym} are the periods of the assigned grating in the (m, n) pixel. The above-mentioned board of gratings is coined a multifacet board and it can be seen schematically in Figure 6.

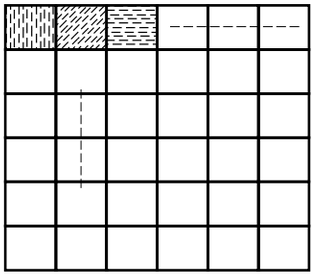

Figure 6. Multifacet board.

The main advantage of the above approach for obtaining the image conversion is that it can provide any desired conversion. Its disadvantage lies in its relatively low resolution of conversion (because within each pixel a grating should be associated and realized). It is important to note that the above-mentioned conversion is obtained in the far field. When monochromatic plane wave illumination is used, the far-field distribution (a Fourier transform) can also be obtained in the back focal plane of a lens (5). In this case, all the formulations previously introduced are valid except that F should substitute z.

Saddle Point Integration Approach

The saddle point integration approach is an approximation technique that achieves a desired image conversion by attaching a phase plate to the image plane and observing the light distribution at the back focal plane of a lens. This is particularly attractive when the desired image conversion (transformation) is an analytic expression.

Let us attach a phase transmission mask having the form of $\exp[i\phi(x, y)]$ to the input image. As previously mentioned, in the back focal plane of a lens, the Fourier transform of the input plane is displayed. Thus:

$$F(u, v) = \iint H(x, y) \exp[i\phi(x, y)] \exp\left[-2\pi i \frac{xu + yv}{\lambda F}\right]\, dx\, dy \tag{22}$$

where $H(x, y)$ is the input image (see the suggested configuration in Fig. 7).

Note that F is the focal length of the lens and $F(u, v)$ is the desired output field distribution. The choice of $\phi(x, y)$ will be

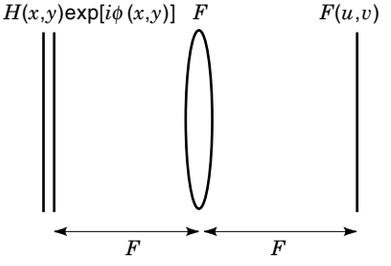

Figure 7. Optical display of the Fourier transform (in the back focal plane of a lens).

determined by the desired transformation. By combining the two exponential terms, the last equation may be rewritten in the form of

$$F(u,v) = \iint H(x,y)\exp[-iq(x,y)]\,dx\,dy \tag{23}$$

where

$$q(x,y) = -\phi(x,y) + \frac{2\pi}{\lambda F}(xu + yv) \tag{24}$$

When the phase term is highly oscillatory, the integration operation can be approximated by the saddle point integration method (6,7), which specifies that the main contribution is provided at the point for which

$$\left.\frac{\partial q(x,y)}{\partial x}\right|_{x_s,y_s} = \left.\frac{\partial q(x,y)}{\partial y}\right|_{x_s,y_s} = 0 \tag{25}$$

Applying these relations leads us to the following set of differential equations:

$$\begin{aligned}\frac{\partial \phi(x,y)}{\partial x} &= \frac{2\pi u}{\lambda F}\\ \frac{\partial \phi(x,y)}{\partial y} &= \frac{2\pi v}{\lambda F}\end{aligned} \tag{26}$$

For instance, when seeking the transformation from Cartesian (x, y) into polar coordinates (lnr, θ) one requires:

$$\begin{aligned}u(x,y) &= \ln r = \frac{1}{2}\ln(x^2+y^2)\\ v(x,y) &= \theta = \tan^{-1}\left(\frac{y}{x}\right)\end{aligned} \tag{27}$$

which leads into

$$\begin{aligned}\frac{\partial \phi}{\partial x} &= \frac{2\pi}{2\lambda F}\ln(x^2+y^2)\\ \frac{\partial \phi}{\partial y} &= \frac{2\pi}{\lambda F}\tan^{-1}\left(\frac{y}{x}\right)\end{aligned} \tag{28}$$

Upon solving for ϕ, one gets the phase mask

$$\phi(x,y) = \frac{2\pi}{\lambda F}\left[\frac{\ln(x^2+y^2)}{2} - y\tan^{-1}\left(\frac{y}{x}\right) - x\right] \tag{29}$$

Note that such a phase mask filter can be easily manufactured by known computer-generated holographic methods (8).

Multistage Approaches

Optical coordinate transformation also can be achieved by using multistage approaches. The use of more than a single stage provides the opportunity to design a system that is based on very simple components. An important advantage of this approach is that it is useful for communications purposes. At present, more and more communications channels rely on optical links, whereas communications switching remains entirely electronic. This combination has two main flaws. The first is the necessity to convert photons to electrons (and vice versa), whereas the second is the limitation of the electronic devices in terms of throughput and bit rate as opposed to the very high capabilities of optical transmission lines (free space, fibers, or waveguides).

Numerous studies concerning all-optical switching and interconnection networks have been carried out. These studies can be divided into three main trends: channeled guided-wave networks, slab waveguide and slab substrate mode interconnections, and three-dimensional free space architectures (9–11). The first two approaches require a physical channel to propagate. The resulting structures are two dimensional and are limited to small-scale systems. Free space architectures, on the other hand, enable three-dimensional arrangements, thus providing the means for a dense system with a large number of parallel communications channels. This type of optical image converter can be used for large-scale free space switches or for compact intracomputer communications systems.

Multistage Interconnect Networks. The most common switching network is based on cross-bar techniques. These structures are simple, wide-sense nonblocking switches. Their major fault lies in the fact that the required number of switching elements increases proportional to N^2 (N = the number of inputs/outputs). One can overcome this deficiency by using multistage interconnection networks (MINs) (12,13). The goal of the MIN is to divide the switch into several cascading stages, each stage consisting of a number of smaller switches that perform a limited switching action. This architecture has three main advantages. First, using the MIN enables one to achieve a large range of implementations by the same switch structure, hence by achieving different connectivity levels (from fully connected switches through rearrangeable nonblocking switches up to strictly nonblocking switches) by using the same switch. The second advantage of the use of MIN structures for implementing the extreme case of strictly nonblocking switches is the requirement of a number of elements proportional only to $N^{1.5}$. As a result, one obtains a significant reduction in the number of elements required for switching a large number of channels. Last, but of no less importance, is the fact that MINs can be implemented recursively. Smaller MINs up to a point where basic, small size switches are used can implement the switches in each stage of the MIN. These advantages of the MIN are accompanied by two disadvantages: the fixed interconnection between the stages and the complicated switching control algorithms.

Multistage Interconnect Networks Classification. One of the basic attributes used to characterize MINs is their connectivity level. The connectivity of the network fits into one of several broad classes. A brief description of these classes is presented hereafter.

1. *Partial Connection.* This class of connectivity means that at least one of the inputs may not be connected to at least one of the outputs. In other words, any two points chosen at random have a probability of less than one of being connected. Even though this type of network has limited function, sometimes-larger networks can be constructed from such subnetworks.
2. *Fully Connected (Also Known as Reduced State).* In this type of network, any single input may be connected to any (arbitrary) output. However, once this is achieved, it may prevent other connections from being imple-

mented. This condition is known as a *block*. Not all permutations are achievable. This type of network is rather popular, due to its relative simplicity. In many cases, the limitation of the reduced states is acceptable.

3. *Rearrangeably Nonblocking*. This type of network allows any permutation of input-to-output connection to be established. However, if a new connection has to be made, some or all of the existing connections have to be disconnected and rearranged, thus introducing a temporary channel interruption until the rearrangement is completed. This type of networks is also one of the more popular types.
4. *Wide-Sense Nonblocking*. This means that new connections may be established without disturbing any of the existing ones.
5. *Strictly Nonblocking*. If a network is strictly nonblocking, any idle input may be connected to any idle output, no matter how many other connections are established, and no matter how the other connections were put up. This type of network is complicated, expensive, and requires a large number of switches.

There are many types of realizations for any of the connectivity types (10). Some of the more popular ones are the Clos network (strictly nonblocking), the crossbar network (wide sense nonblocking), and the Benes network (rearrangeably nonblocking). An interesting type of fixed interconnection is the Omega network (perfect shuffle). Using the perfect shuffle to connect layers of switches, one may get networks from partially connection through wide-sense nonblocking, depending on the number of layers applied. The reduced (fully connected) and the nonreduced (rearrangeably nonblocking) networks are among the achievement capabilities of this type of connection.

The one-dimensional perfect shuffle (taking its name from the shuffling of a pack of cards) method is carried as follows: the input is divided into two halves, and thereafter the first half is connected to the odd outputs and the second half to the even ones in sequence. The result is an interlaced connection. The result for eight inputs/outputs is depicted in Figure 8. If two-dimensional MINs are to be implemented, then a two-dimensional perfect shuffle should be used. The two-dimensional extension of the perfect shuffle is straightforward, along the same lines.

Another important types of fixed interconnections are the cross-over and the Banyan networks. Those networks for eight input/outputs are illustrated in Figure 9.

A 2 × 2 Optical Switch. The basic building block for the MINs is the 2 × 2 free space optical switch (FSOS). This switch is also known as bypass-exchange switch. A certain implementation of such switch is displayed in Figure 10.

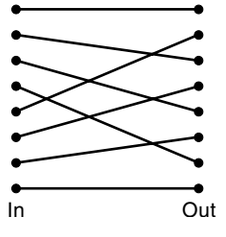

Figure 8. Perfect shuffle for eight inputs/outputs.

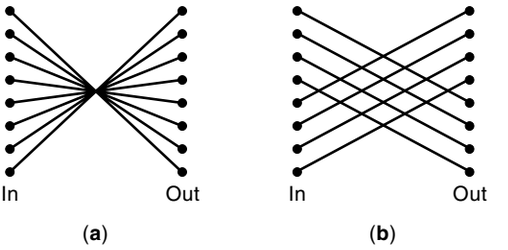

Figure 9. (a) Crossover network. (b) Banyan network, for eight inputs/outputs.

Two incoming signals A and B are set to linear polarization in orthogonal directions. Both signals enter the calcite crystal with polarization directions aligned with the crystal's orientation (ordinary and extraordinary). The crystal length provides a displacement that equals the distance between inputs A and B, guaranteeing that both signals emerge from the calcite as one ray with two orthogonal polarizations, representing signals A and B. The orthogonally polarized signals pass through a controllable $\lambda/2$ device. If the device is activated, the two orthogonal signals will undergo a 90° rotation, so that the two signals A and B will exchange their polarization state. The signals will then split by the second calcite crystal. In view of the rotated polarizations, the two signals A and B, emerging from the switch in an exchange position, will interchange. Not activating the $\lambda/2$ device, the ray will pass through without undergoing polarization rotation, and the two signals A and B will emerge after the second calcite, in the same course as they entered the switch.

Basic 4 × 4 Optical Switch. The 4 × 4 FSOS is the cornerstone for large MIN systems. The reduced (fully connected blocking) 4 × 4 FSOS consists of four independently controlled bypass-exchange switches. The 4 × 4 FSOS consists of four 2 × 2 switches depicted in Figure 11. It is simply designed and highly symmetric, thus accomplishing a small-scale switch, with easy alignment and high light efficiency, while using low number of switches.

The 4 × 4 FSOS is a two-stage omega MIN, fully connected switch (i.e., enabling one single input to connect to any output). Yet, some connections will be impossible to create if other connections already exist (Fig. 12). Furthermore, it is seen that the 4 × 4 FSOS implements the two-stage MIN in a two-dimensional structure. The points mentioned above enhance the certainty that the 4 × 4 FSOS is a suitable solution for a small-scale switch of larger three-dimensional optical MINs.

Comparison Between Approaches

The main advantage of the multifacet approach is its ability to fulfill any desired coordinate transformation, which results in any desired image conversion in a relatively simple optical setup. However, the approach has two main disadvantages. Since within each image a facet with an appropriate grating must be inserted, the number of channels that can be addressed is restricted due to technological production limita-

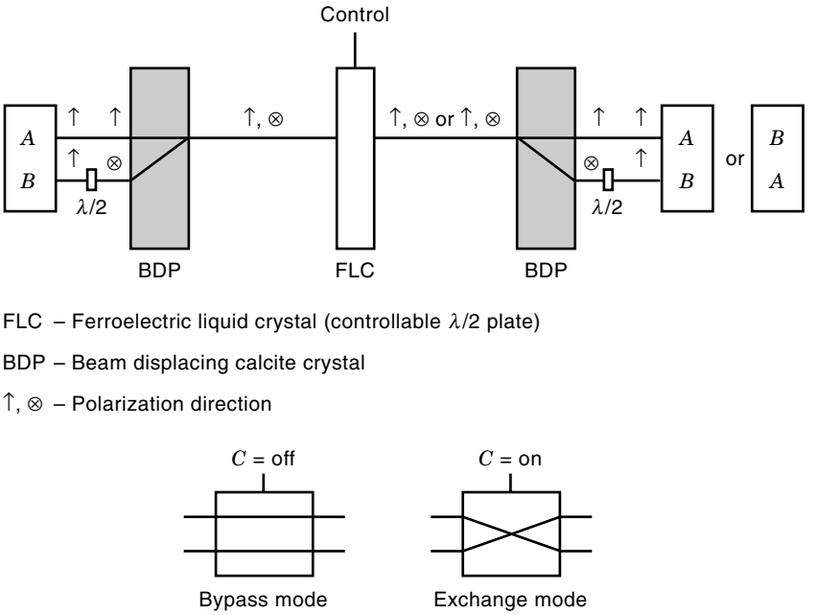

Figure 10. Bypass-exchange switch.

tions. Nevertheless, the production is quite difficult even when the spatial resolution is low.

The saddle point integration requires a simpler phase mask, which allows obtaining higher spatial resolution of coordinate transformation and easier fabrication. However, the main disadvantage of this approach, besides its being only an approximation, is that not every coordinate transformation relation may be realized. Reviewing the previously mentioned equations reveals that an exact solution does not always exist.

The multistage approach is a very promising recently established technique. This approach allows both fast and highly resolved image conversions to be achieved. Because it is so new, it has not yet been implemented compactly and efficiently, but future technological progress will no doubt solve this drawback.

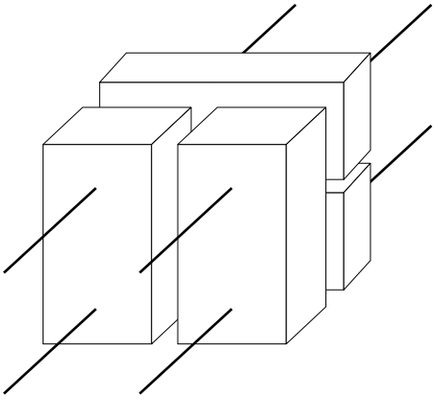

Figure 11. 4 × 4 FSOS. Each rectangle represents a bypass-exchange switch.

OPTICAL COORDINATE TRANSFORMATIONS—NUMERICAL APPROACHES FOR MASK COMPUTATION

Ping-Pong Based Algorithms

Complex amplitude masks are often required for optical information processing and coordinate transformation. Because these masks are hard to fabricate and inefficient as a result of amplitude (absorbing) variations, ways to avoid the use of such elements by substituting them with phase-only masks are considered. Numerical approaches for doing so, such as a ping-pong algorithm, have become very common recently due to the increasing computational ability of digital computers.

One of the basic ping-pong techniques is the Gerchberg–Saxton (G–S) algorithm, which was invented and used for various applications such as super resolution, phase retrieval, and beam shaping (14–21). It is based on numerical iterations for determining the necessary phase function $\phi(x, y)$ that can generate the desired distribution at the output plane $(\bar{x}, \bar{y})$. The suggested optical setup used for beam shaping implementations is demonstrated in Figure 13. As illustrated in this figure, the input field distribution is multiplied by a spatial phase-only filter, $\exp[i\phi(x, y)]$ and Fourier transformed using the optical setup previously seen in Figure 7.

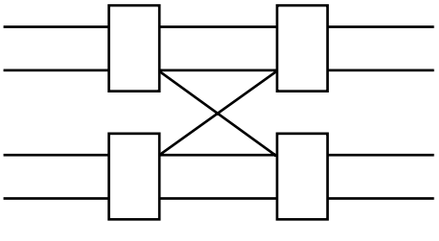

Figure 12. Two-stage omega 4 × 4 MIN.

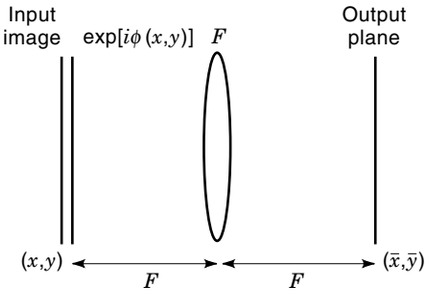

Figure 13. Gerchberg–Saxton algorithm for beam shaping.

The goal is to achieve a desired amplitude distribution in the output plane. Once this is achieved, after many iterations, the final desired phase is generated with a second filter placed in the output plane. The iterative algorithm, which is applied for calculating the spatial phase filter, is illustrated in Figure 14. Its goal is to determine $\phi(x, y)$ such that it will meet with the desired output amplitude distribution under an input amplitude distribution constraint.

For the first iteration in the iterative algorithm described in Figure 14, a random phase $\phi_{in}(x, y)$ is chosen. A new function $f(x, y) = A_{in}(x, y) \exp[i\phi_{in}(x, y)]$ is defined, where $A_{in}(x, y)$ is the actual input amplitude distribution (a constraint). The output plane serves as a certain predetermined transformation of the input plane. For instance, it is common to obtain the output in the Fourier plane. In this case a fast Fourier transform (FFT) of $f(x, y)$ may be performed, in order to shift to the output plane and to examine the field distribution there:

$$F(\bar{x}, \bar{y}) = \int f(x, y) \exp[-2\pi i(x\bar{x} + y\bar{y})]\, dx\, dy = \tilde{A}_{out}(\bar{x}, \bar{y}) \exp[i\phi_{out}(\bar{x}, \bar{y})] \quad (30)$$

The next step is to replace $\tilde{A}_{out}(\bar{x}, \bar{y})$ by the constraint for the output amplitude distribution $A_{out}(\bar{x}, \bar{y})$. After performing an inverse FFT over the result (we shift again back to the input plane), the obtained phase becomes the input phase $\phi_{in}(x, y)$ for the second iteration. The process is repeated until convergence occurs. The input spatial phase filter is $\exp[i\phi_{in}(x, y)]$, as seen in Figure 13. Thus, if the input amplitude distribution

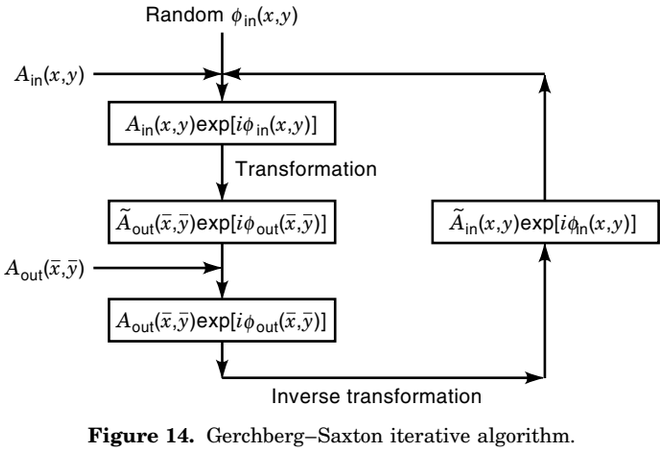

Figure 14. Gerchberg–Saxton iterative algorithm.

is $A_{in}(x, y)$, the amplitude distribution obtained in the Fourier plane will be approximately the constrained amplitude distribution $A_{out}(\bar{x}, \bar{y})$. Note that if the input field distribution has a phase of $\phi_g(x, y)$ in addition to the amplitude $A_{in}(x, y)$, then the input phase filter will be $\exp[-i\phi_g(x, y) + i\phi_{in}(x, y)]$.

The phase obtained in the output plane is $\phi_{out}(\bar{x}, \bar{y})$. Once the output amplitude constraint is achieved, the phase of the output field distribution can be corrected, if necessary, by another phase-only filter. The phase filter that has to be placed at the output plane is $\exp[-i\phi_{out}(\bar{x}, \bar{y}) + i\phi_d(\bar{x}, \bar{y})]$ where $\phi_d(\bar{x}, \bar{y})$ is the constraint for the output phase.

As previously mentioned, a Fourier transform is not the only transformation that ties the input and the output plane. Other possible transformations that are often used are the fractional Fourier transform and the Fresnel transform (22–24). The main difference between the various types of transformations is the residual error for the image conversion obtained in the output plane and the rate of the numerical algorithmic convergence.

Simulated Annealing Algorithms

The simulated annealing algorithms (25) are a very general type of algorithm used for image conversion for many other uses, including a comparison condition. The idea behind the simulated annealing is simple; it was taken from physical processes existing within nature. For instance, when a material is slowly cooled its molecular structure becomes more and more organized by the movement of its particles. However, this movement is reduced monotonically with the decrease of the temperature. Usually the decrease is exponential with temperature (which is proportional to the time axis):

$$D = D_0 \exp\left(-\frac{\alpha}{T}\right) \quad (31)$$

where D is the probability to apply the rule of order and to switch the position of two states, T is the temperature, and α is a constant.

If one desires to organize an image or an array according to a certain rule of order, then to obtain faster convergence that will not converge to a local minima the rule of order is applied according to a certain probability of distribution that changes time. The change in time of the probability to apply the rule of order may be exponential (remember that $T = T(t)$, where t is the time base), or it may have any other form of monotonic decrement with time. At the end of the process, the probability for a change is close to zero. This property allows a moderate sorting of the process, which prevents us from converging to local undesired minima.

Simulated annealing is a very promising algorithm, not yet used sufficiently in optical image conversions.

APPLICATIONS

Beam Forming and Shaping

In this section we illustrate the use of a modified numerical Gerchberg-Saxton–based algorithm to obtain an efficient image conversion. To provide the reader with a more substantial grip on the importance of optical image converters, we detail the following application and explore it in a fundamental manner.

Over the years, many efforts at beam-shaping conversion have been made. A popular example of beam shaping consists of generating one- or two-dimensional arrays of equal-intensity light spots. In 1971 Dammann and Gortler tried to obtain such beam shaping in the form of multiple images from one input object (26). They used periodic special gratings, later coined *Dammann gratings,* to achieve their goal. Dammann gratings are simple binary phase gratings used to generate arrays of equal-intensity light spots. Later, Dammann and Klotz explained the theory behind the Dammann gratings in greater detail (27).

Killat et al. (28) and Veldkamp et al. (29) suggested different uses of the Dammann gratings. A feasibility study of Dammann gratings and their important parameters has been done as well (30). Interest in the Dammann gratings increased lately, mainly due to new developments in optical digital computing and infrared computer communications where arrays of light spots are needed to provide optical beam sources for a large number of synchronized logic devices. But the reason that the Dammann gratings were, and still are, very popular is due not only to their applicability but also to the fact that they are actually binary phase gratings. This provides high efficiency in view of the high throughput of light energy. The binarization enables the use of fabrication techniques, such as reactive ion etching and photolithography, which have become standard processes in VLSI technology.

Unfortunately, Dammann gratings have some serious drawbacks. They cannot generate an arbitrary array of light spots, being restricted to only an odd number of spots along each axis and equal spacing between two neighboring spots. Furthermore, Dammann gratings are restricted to structures with transparencies functions, $t(x, y)$, that can be separated into the spatial coordinates x and y:

$$t(x, y) = t_1(x)t_2(y) \tag{32}$$

Hence they cannot produce, for example, light spots arranged in a circular unequally spaced array. If one tries to generate an array of more than 40×40 spots, problems with the computation of the gratings become dominant (30). Finally, even though Dammann gratings are binary phase filters, their overall efficiency is relatively low in most cases.

The following approach for the design of a beam-shaping generator is based upon the numerical Gerchberg–Saxton (G–S) algorithm (31). The one and the most common application is beam shaping while the desired beam shape is obtained in either the Fourier or in the Fresnel planes.

At this point we would like to mention that the discussion carried in this subsection is general and the proposed method may be used for generating other desired amplitude and phase distributions. In our application example we concentrate on the case of an arbitrary array generator.

Light-Efficient Array Illuminator. The optical setup proposed for implementing a light-efficient array illuminator is given in Figure 15. The setup includes phase-only elements and thus provides maximum throughput of light energy, which yields high efficiency.

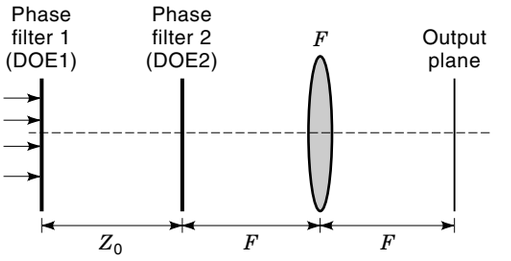

Figure 15. Optical setup for implementing array illuminator.

Assuming that the input field distribution is denoted by $A_{\text{in}}(x', y')$, the field distribution behind the first diffractive optics element (DOE1) is

$$f(x', y') = A_{\text{in}}(x', y') \exp[i\phi_1(x', y')] \tag{33}$$

where $\phi_1(x', y')$ is an arbitrary plane distribution.

According to this setup, the field propagates in free space from the first DOE (DOE1) to the second DOE (DOE2) over a distance Z_0. At that point, right before DOE2, the field distribution $g(x, y)$ can be mathematically calculated by using the Fresnel diffraction integral:

$$g(x, y) = \frac{\exp\left(\frac{2\pi i Z_0}{\lambda}\right)}{i\lambda Z_0} \iint f(x', y') \exp\left\{\frac{2\pi i Z_0}{\lambda}[(x - x')^2 + (y - y')^2]\right\} dx'\, dy' \tag{34}$$

Right behind the second phase-only spatial filter the field is

$$s(x, y) = g(x, y) \exp[i\phi_2(x, y)] \tag{35}$$

The output plane and the DOE2 plane are connected by a Fourier transform relation, so that

$$S(u, v) = \iint s(x, y) \exp\left[\frac{-2\pi i}{\lambda F}(xu + yv)\right] dx\, dy \tag{36}$$

One strives that $S(u, v)$ be as similar as possible to the desired output shape $D(u, v)$:

$$D(u, v) = A_{\text{out}}(u, v) \exp[i\phi_{\text{out}}(u, v)] \tag{37}$$

Denoting by $d(x, y)$ the desired field distribution right behind DOE2, this function is the inverse Fourier transform of $D(u, v)$ and can be calculated as

$$d(x, y) = C \iint D(u, v) \exp\left[\frac{2\pi i}{\lambda F}(xu + yv)\right] du\, dv \tag{38}$$

where C is a constant.

The unknown parameters in the proposed configuration are the distance between the two diffractive optics filters (Z_0) and the phase-only spatial filter distributions ϕ_1 and ϕ_2, whose functions are to be calculated. Therefore, the following questions have to be answered:

How to determine the distance Z_0

How to calculate the two phase only spatial filters

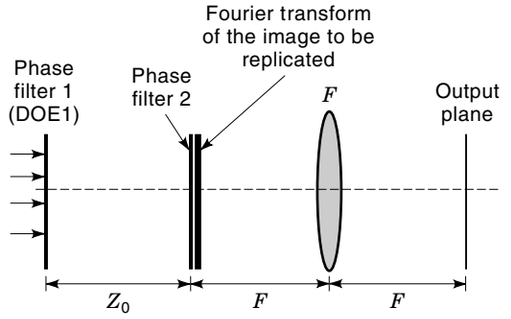

Figure 16. Optical setup for the creation of image replication.

The next section provides answers to these questions.

One should note that the optical implementation of an efficient array illuminator can be also used for obtaining image replication as shown in Figure 16. The Fourier transform of the object f_{in} that we wish to replicate is placed in front of DOE2. At the output of the system, the convolution between an array of spots and the object f_{in} is obtained; replication is thus generated.

Beam-Shaping Generator—Mathematical Analysis. The desired output field distribution $D(u, v)$ should be obtained at the back focal plane of the lens. Therefore, its inverse Fourier transform, $d(x, y)$, should appear at the front focal plane of the lens. $d(x, y)$ can be expressed as

$$d(x, y) = A_d(x, y) \exp[i\phi_d(x, y)] \tag{39}$$

Thus, for a given input field distribution, $A_{in}(x', y')$, one should calculate the first phase only spatial filter $\exp[i\phi_1(x', y')]$ that will generate at a distance Z_0 from that filter the $A_d(x, y)$ distribution.

The second phase-only spatial filter should provide the desired phase of $d(x, y)$. The illuminating source and the first DOE $[\phi_1,(x', y')]$, provide at a distance Z_0:

$$g(x, y) = A_0(x, y) \exp[i\phi_0(x, y)] \tag{40}$$

Since $\phi_1(x', y')$ is computed in such a way that

$$A_d(x, y) = A_0(x, y) \tag{41}$$

one obtains that the second phase-only filter $\phi_2(x, y)$ should thus satisfy:

$$\phi_2(x, y) = \phi_d(x, y) - \phi_0(x, y) \tag{42}$$

To calculate the first filter, the G–S iterative algorithm is used. The flowchart that illustrates the procedure is similar to the one of Figure 14, whereby the transform is the Fresnel transform in this case. In most cases, adequate convergence occurs after hundreds of iterations. This thus provides the phase mask $\exp[i\phi_1(x', y')]$ represented by the first DOE placed in the setup of Figure 15.

The free space propagation distance, Z_0, between the two DOEs depends upon two major factors: the input amplitude distribution $A_{in}(x, y)$ and the desired output field distribution $D(u, v)$. For specific functions $A_{in}(x, y)$ and $D(u, v)$, several values of Z_0 may lead to an optimal convergence, hence flexibility exists in choosing the parameter Z_0. Note that the value of Z_0 affects the rate of convergence of the G–S iterative algorithm.

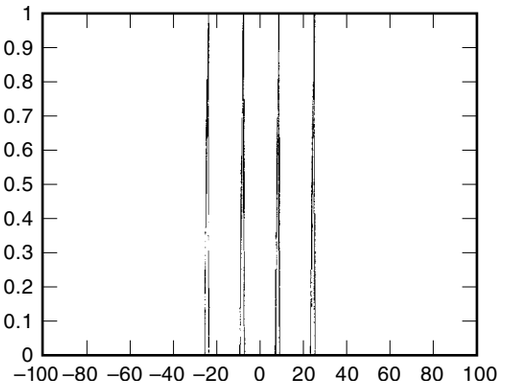

Figure 17. The desired beam shape (four equally spaced impulses).

Computer Simulations. To demonstrate the ability of this application, we present several designs for the generation of a two-dimensional array of light spots that can be mathematically expressed by

$$D(u, v) = \sum_n \sum_m A_{m,n} \delta(x - x_m, y - y_n) \tag{43}$$

where $D(u, v)$ is the desired output field distribution and $A_{m,n}$ is the amplitude of a light spot located in the spatial coordinate (x_m, y_n). Thus, behind DOE2 a reconstruction of a series of plane waves is needed.

The first simulation treats the generation of an array with an even number of equally intense light spots. This aim is unachievable by conventional means (26,27). The desired beam shape is presented in Figure 17 and consists of four equally spaced impulses. Figure 18 shows the results achieved after 100 iterations of the G–S procedure. An extremely close match is observed between the two figures.

The squared error between the obtained and the desired result is 7.39×10^{-5}. Furthermore, the energy loss was found to be only 1.4×10^{-5} of the total energy; that is, an overall

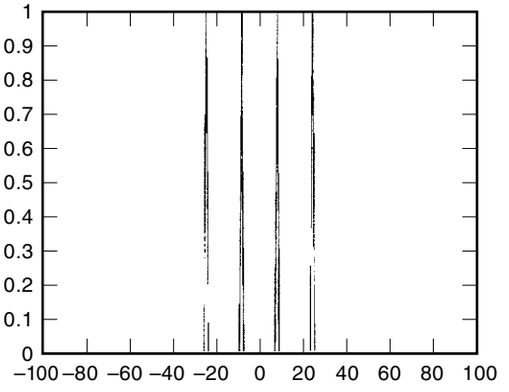

Figure 18. The obtained beam shape (where Fig. 17 is the goal).

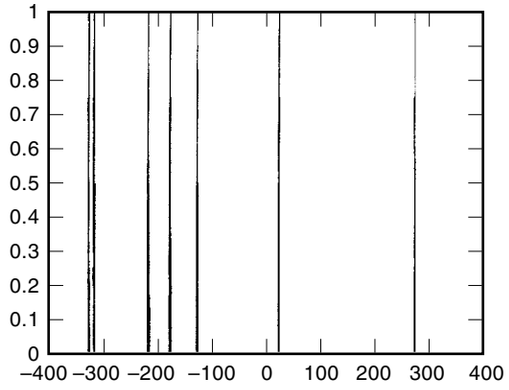

Figure 19. The desired beam shape (an asymmetric array of seven impulses).

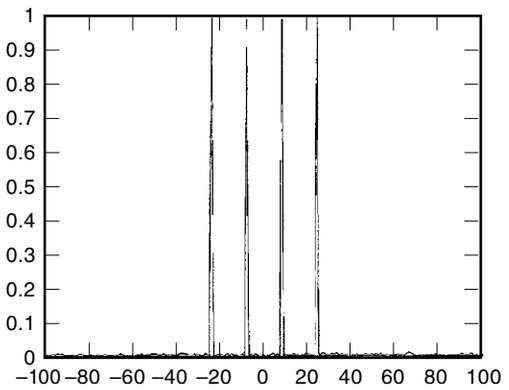

Figure 21. The obtained beam shape for Fig. 17 when additive noise is introduced.

efficiency of 0.999986 was achieved. Note that we ignored reflection and propagation losses of the illuminator.

The second simulation is aimed at producing an asymmetric array of equally intense light spots with different spacing between the spots. Figure 19 shows the desired beam shape and Figure 20 presents the results achieved by the suggested procedure after 100 iterations of the G–S algorithm. The squared error in this case is 6×10^{-3} and the overall efficiency is 0.999146. The small error in both cases illustrates a good convergence of the algorithm and uniformity of the spots. Note that simulations performed with a larger number of iterations (of the G–S iterative algorithm) provide even better results.

We now investigate the behavior of the suggested optical setup in the presence of noise (added to the phase functions of the masks) to test the ruggedness of the method. White Gaussian noise (WGN), with zero mean and a standard deviation of two degrees, was added to the phase function of the masks. Figure 21 presents the results obtained when an array of four equal intensity light spots is generated under the presence of such noise. The overall efficiency in this case is 0.990637. Figure 22 presents the obtained results whereby an asymmetric array of seven equal-intensity light spots is generated in the presence of noise. The overall efficiency in this case is 0.989680.

In addition to the high efficiency and flexibility, the suggested method is also advantageous (over the conventional Dammann plate) in handling noise embedded in the phase of the masks. This overcomes the restriction presented in Ref. 30, where the sensitivity to noise is presented as a significant drawback.

Optical Signal Processing. The techniques presented herein also play a major role in the optical signal-processing field of research. Its most significant importance is in implementation of different optical transformations used for image enhancement and noise removal, for superresolution, and for invariant pattern recognition. The following sections briefly overview this type of application for image converters.

Image Enhancement and Noise Removal. Previous researches have demonstrated the importance of different transformations for image enhancement. Many of those transformations are based upon image converters. For instance, the Mellin transform (32) is a well-known transformation used in radar image-processing applications as well as in optical scale-invariant pattern recognition. This transform realizes the conversion from (x, y) into $(\ln r, \theta)$ coordinates. The image conversion using the coordinate transformation is performed by the techniques described herein.

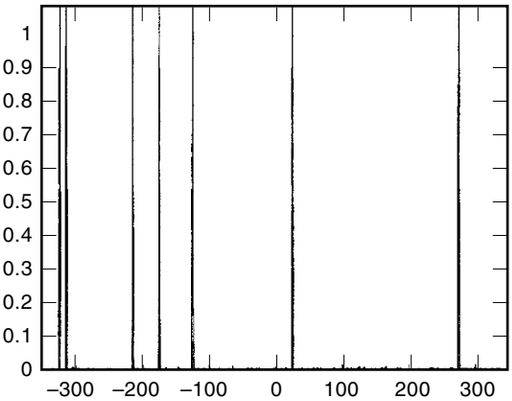

Figure 20. The obtained beam shape (where Fig. 19 is the goal).

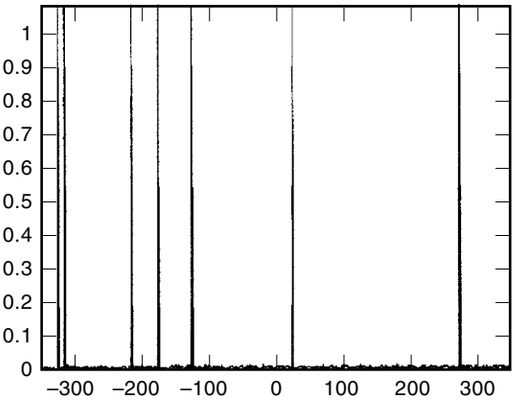

Figure 22. The obtained beam shape for Fig. 19 when additive noise is introduced.

Superresolution. Superresolution is perhaps the most fundamental research topic in optics (33,34). The meaning of this term is to improve the spatial resolution seen by an optical imaging device. Resolution degradation is caused by the finite apertures of the imaging systems (diffraction resolution restriction) and by the finite pixel size in CCD sensing devices. The way to overcome the diffraction restriction is to synthetically enlarge the aperture of the lens. This may be done by methods that multiplex the spatial information existing within the input image, transmitting it throughout the aperture and then demultiplexing it back again. The means of proper multiplexing and demultiplexing often include sophisticated Dammann gratings that create the desired image conversions (35,36).

Invariant Pattern Recognition. Invariant pattern recognition is most important in computer vision and automatic target-detection systems. Invariant pattern recognition should allow detection of not only the undistorted reference image but also when it is scaled, projected or rotated (32,37,38), or embedded in noise (39). If, for instance, we examine the scale invariant case, it is clear that the invariance may be achieved by performing a Cartesian to $(\ln r, \theta)$ coordinate transformation (40). If the input object is scaled by a factor of a: $r \rightarrow a \cdot r$, then the coordinate transformation will result by a lateral shift of the transformed image:

$$\ln(ar) = \ln a + \ln r \tag{44}$$

Because the recognition is usually based upon a correlation, which is a shift-invariant operation, scale-invariant pattern recognition is obtained. This is because we sacrifice the shift-invariance property of the overall system for achieving the scale-invariance property. The desired coordinate transformation may be obtained by the above-discussed techniques.

A similar discussion may be done for projection- or rotation-invariant pattern recognition. Projection invariance means obtaining invariant recognition for the reference object and for the reference object being scaled only in one of the axes x or y. In this case a coordinate transformation of $(\ln x, \ln y)$ may be very efficient because scales in x or in y result in shifts. Due to the shift-invariance property of the correlation operation, a projection invariant recognition may be achieved.

Coherent and Incoherent Light Processing

This subsection discusses the application of optical image converters in incoherent light processing. Optical information processing became feasible when Vander Lugt (41) invented what is nowadays called the 4-f correlator (Fig. 23). In this system a two-dimensional Fourier transformation is obtained via a lens, a filter is then placed in the Fourier plane, and then another Fourier transform module leads to the output plane. Thus, convolution or correlation operations between the input and the impulse response of the filter may be obtained. A somewhat different setup for achieving the same goal is known as the joint-transform correlator (JTC) (42,43), which does not require any spatial filter, but a simultaneous presentation of the reference and the image side by side in the input plane. Thus it provides some advantages compared with the conventional 4-f configuration since there is no need for a spatial filter that should be positioned with high accuracy. The JTC configuration is based on presenting simultaneously two patterns at the input plane one beside the other. The JTC (Fig. 24) contains two steps: The first step is actually a Fourier transformer obtained by a lens followed by a square law converter device (a device that converts field distribution to amplitude distribution). The result is fed back to the input plane (possibly by computer interface). The second step is another Fourier transformation such that in the output plane at first diffraction orders, correlation between the input and the reference patterns is obtained.

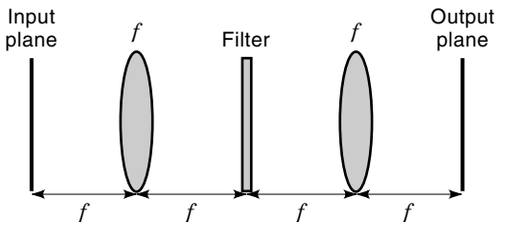

Figure 23. 4-*f* correlator.

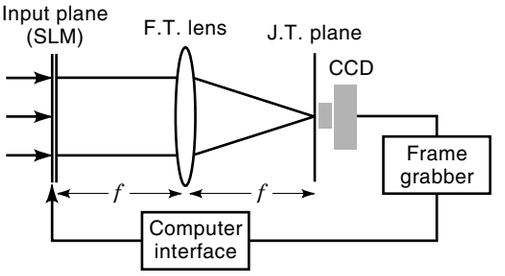

Figure 24. Joint transform correlator.

Several approaches for implementing the square-law conversion are in use, such as photographic-film (43), spatial light modulator (SLM), and liquid crystal light valve (LCLV) (44,45). Incoherent processing started to be popular when it was shown that the 4-f system performs a convolution/correlation operation between the input intensity distribution and the intensity of the filter's impulse response, when illuminated by a quasimonochromatic, spatially incoherent light (46).

The intrinsic advantages and applications of using spatially incoherent light for optical signal processing have been intensively discussed (47,48). For the JTC, a white light configuration has been suggested (49). In the following, a spatially incoherent JTC implementation that provides various advantages comparing with other optical processors is suggested. The suggested implementation is based on the shearing interferometer (50).

By using the shearing interferometer, which includes a corner prism, the Hartley transform is obtained at the output plane (51) following the optical configuration of Figure 25.

The Hartley transform was achieved for either spatially incoherent or coherent illumination. Such a setup, due to the beam splitter, divides the light coming from the input pattern into two paths. One optical path contains the information of the original input reflected from a mirror. The other path is the original input that was returned from the corner prism. Thus the original pattern rotated by 180° [$g(x, y)$ becomes

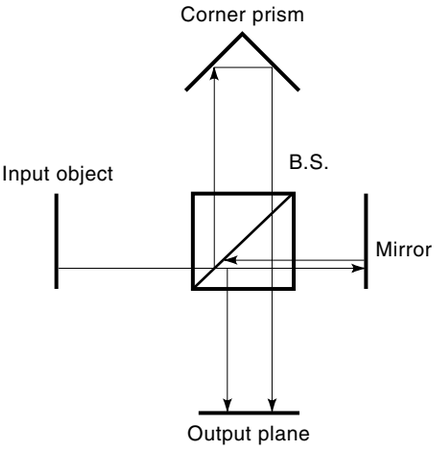

Figure 25. The optical setup to implement the Hartley transform.

$g(-x, -y)$]. Thus, in both paths simple optical image converters were used to achieve the Hartley transform, which is an image conversion by itself.

The two paths recombined together with the beam splitter. Every point at the object plane is split to two diffraction patterns according to the two paths. These paths interfere among themselves in spite of the fact that the preliminary illumination was spatially incoherent, since both paths are originated in the same spatial spot in the input pattern.

In sum, the proposed scheme is based on using coherent light for finding the joint spectrum by performing a Fourier transform using a lens, mechanically breaking the spatial coherence by placing a rotated diffuser, and then performing the second Fourier-like transform (the Hartley transform) with the incoherent shearing interferometer. The final configuration is simple and does not need any electrical conversion. Thus it is fast and provides high spatial resolution.

BIBLIOGRAPHY

1. J. K. Anil, *Fundamentals of Digital Image Processing,* Englewood Cliffs, NJ: Prentice-Hall, 1989.
2. W. K. Pratt, *Digital Image Processing,* New York: Wiley, 1978.
3. S. K. Case, P. R. Haugen, and O. J. Loberge, Multifacet holographic optical elements for wave front transformations, *Appl. Opt.,* **20**: 2670–2675, 1981.
4. D. Mendlovic and H. Ozaktas, Optical coordinate transformation methods and optical interconnection architectures, *Appl. Opt.,* **32**: 5119–5124, 1993.
5. J. W. Goodman, *Introduction to Fourier Optics,* 2nd ed., New York: McGraw Hill, 1996.
6. L. B. Felsen and N. Marcuvitz, *Radiation and Scattering of Waves,* Englewood Cliffs, NJ: Prentice-Hall, 1973, p. 421.
7. O. Bryngdahl, Geometrical transformations in optics, *J. Opt. Soc. Amer.,* **64**: 1092–1099, 1974.
8. A. W. Lohmann and D. P. Paris, Binary Fraunhofer holograms, generated by computer, *Appl. Opt.,* **6**: 1739–1749, 1967.
9. K. M. Johnson, M. R. Surette, and J. Shamir, Optical interconnection network using polarization-based ferroelectric liquid crystal gates, *Appl. Opt.,* **27**: 1727–1733, 1988.
10. H. Yamazaki and S. Fukushima, Holographic switch with a ferroelectric liquid crystal spatial light modulator for a large scale switch, *Appl. Opt.,* **35**: 8137–8143, 1995.
11. D M. Marom and D. Mendlovic, Compact all-optical bypass-exchange switch, *Appl. Opt.,* **35**: 248–253, 1996.
12. J. E. Midwinter, *Photonics in Switching,* Vols. 1 and 2, New York: Academic Press, 1993.
13. H. Ozaktas and D. Mendlovic, Multi-stage interconnection architecture with least possible growth system size, *Opt. Lett.,* **18**: 296–298, 1993.
14. E. Noel, R. R. Khan, and H. S. Dhadwal, Optical implementation of a regularized Gerchberg iterative algorithm for super-resolution, *Opt. Eng.,* **32**: 2866–2871, 1993.
15. R. W. Gerchberg, Super-resolution through error energy reduction, *Opt. Acta,* **21**: 709–720, 1974.
16. G. Z. Yang et al., Gerchberg-Saxton and Yang-Gu algorithms for phase retrieval in a nonunitary transform system: A comparison, *Appl. Opt.,* **33**: 209–218, 1994.
17. D. F. McAlister et al., Optical phase retrieval by phase-space tomography and fractional-order Fourier transforms, *Opt. Lett.,* **20**: 1181, 1995.
18. M. Hedley, H. Yan, and D. Rosenfeld, A modified Gerchberg-Saxton algorithm for one-dimensional motion artifact correction in MRI, *IEEE Trans. Signal Processing,* **SP-39**: 1428–1432, 1991.
19. R. W. Gerchberg and W. O. Saxton, Phase determination from image and diffraction plane pictures in the electron microscope, *Optik,* **34**: 277, 1971.
20. R. W. Gerchberg and W. O. Saxton, A practical algorithm for the determination of phase from image and diffraction plane pictures, *Optik,* **35**: 227, 1972.
21. R. W. Gerchberg and W. O. Saxton, in P. W. Hawkes (ed.), *Image Processing and Computer Aided Design in Electron Optics,* New York: Academic Press, pp. 66–81.
22. D. Mendlovic and H. M. Ozaktas, Fractional Fourier transforms and their optical implementation: I, *J. Opt. Soc. Am. A,* **10**: 1875–1881, 1993.
23. A. W. Lohmann, Image rotation, Wigner rotation, and the fractional Fourier transform, *J. Opt. Soc. Am.,* **10**: 2181–2186, 1993.
24. Z. Zalevsky, D. Mendlovic, and R. Dorsch, The Gerchberg–Saxton algorithm applied in the fractional Fourier or the Fresnel domains, *Opt. Lett.,* **21**: 842–844, 1996.
25. S. Kirkpatrick, C. D. Gelatt Jr., and M. P. Vecchi, Optimization by simulated annealing, *Science,* **220**: 671–680, 1983.
26. H. Dammann and K. Gortler, High-efficiency in-line multiple imaging by means of multiple phase holograms, *Opt. Commun.,* **3**: 312–315, 1971.
27. H. Dammann and E. Klotz, Coherent-optical generation and inspection of two-dimensional periodic structures, *Opt. Acta,* **24**: 505–515, 1977.
28. U. Killat, G. Rabe, and W. Rave, Binary phase gratings for star couplers with high splitting ratio, *Fiber Integr. Opt.,* **4**: 159–167, 1982.
29. W. B. Veldkamp, J. R. Leger, and G. J. Swanson, Coherent summation of laser beams using binary phase gratings, *Opt. Lett.,* **11**: 303–305, 1986.
30. J. Jahns et al., Dammann gratings for laser beam shaping, *Opt. Eng.,* **28**: 1267–1275, 1989.
31. D. Mendlovic et al., High efficiency arbitrary array generator, *Appl. Opt.,* **35**: 6875–6880, 1996.
32. D. Mendlovic, E. Marom, and N. Konforti, Shift and scale invariant pattern recognition using Mellin radial harmonics, *Opt. Commun.,* **67**: 172, 1988.
33. W. Lukosz, Optical systems with resolving powers exceeding the classical limit, *J. Opt. Soc. Am.,* **56**: 1463–1472, 1966.

34. W. Lukosz, Optical systems with resolving powers exceeding the classical limit II, *J. Opt. Soc. Am. A,* **57**: 932, 1967.
35. D. Mendlovic et al., One dimensional superresolution optical system for temporally restricted objects, *Appl. Opt.,* **36**: 2353–2359, 1997.
36. D. Mendlovic et al., Two dimensional superresolution optical system for temporally restricted objects, *Appl. Opt.,* **36**: 6687–6691, 1997.
37. D. Mendlovic, N. Konforti, and E. Marom, Shift and projection invariant pattern recognition using logarithmic harmonics, *Appl. Opt.,* **29**: 4784–4789, 1990.
38. Y. H. Hsu and H. H. Arsenault, Optical pattern recognition using circular harmonic expansion, *Appl. Opt.,* **21**: 4016–4019, 1982.
39. E. Marom and H. Inbar, New interpretations of Wiener filters for image recognition, *J. Opt. Soc. Am. A,* **13**: 1325–1330, 1996.
40. D. Mendlovic, N. Konforti, and E. Marom, Scale and projection invariant pattern recognition, *Appl. Opt.,* **28**: 4982–4986, 1989.
41. A. Vander Lugt, Signal detection by complex spatial filtering, *IEEE Trans. Inform. Theory,* **IT-109**: 139–146, 1964.
42. J. E. Rau, Detection of differences in real distributions, *J. Opt. Soc. Am.,* **56**: 1490–1494, 1966.
43. C. S. Weaver and J. W. Goodman, A technique for optically convolving two functions, *Appl. Opt.* **5**: 1248–1249, 1966.
44. F. T. S. Yu et al., Adaptive real-time pattern recognition using a liquid crystal TV based joint transform correlator, *Appl. Opt.,* **26**: 1370–1372, 1987.
45. F. T. S. Yu and X. J. Lu, A real time programmable joint transform correlator, *Opt. Commun.,* **52**: 10–16, 1984.
46. A. W. Lohnmann and H. W. Werlich, Incoherent matched filter with Fourier holograms, *Appl. Opt.,* **7**: 561–563, 1968.
47. H. Bartelt, S. K. Case, and R. Hauck, Incoherent optical processing, in H. Stark (ed.), *Applications of Optical Fourier Transforms,* Orlando, FL: Academic Press, 1982.
48. I. Glaser, Information processing with spatially incoherent light, *Prog. Opt.,* **24**: 389–509, 1987.
49. F. T. S. Yu and Y. S. Cheng, White light joint transform correlator, *Opt. Lett.,* **15**: 192–194, 1990.
50. S. Wang and N. George, Fresnal zone transforms in spatially incoherent illumination, *Appl. Opt.,* **24**: 842–850, 1985.
51. R. N. Bracewell et al., Optical synthesis of the Hartley transform, *Appl. Opt.,* **24**: 1401–1402, 1985.

ZEEV ZALEVSKY
DAVID MENDLOVIC
GAL SHABTAY
EMANUEL MAROM
Tel Aviv University